

## Supporting Information

### **Tuning the Electrocatalytic Oxygen Reduction Reaction Activity and Stability of Shaped-Controlled Pt-Ni Nanoparticles by Thermal Annealing – Elucidating the Surface Atomic Structural and Compositional Changes**

*Vera Beermann,<sup>a</sup> Martin Gocyla,<sup>b</sup> Stefanie Kühl,<sup>a</sup> Elliot Padgett,<sup>c</sup> Henrike Schmies,<sup>a</sup> Mikaela Görlin,<sup>a</sup> Nina Erini,<sup>a</sup> Meital Shviro,<sup>b</sup> Marc Heggen,<sup>b</sup> Rafal E. Dunin-Borkowski,<sup>b</sup> David A. Muller,<sup>c</sup> and Peter Strasser<sup>a\*</sup>*

<sup>a</sup> *Electrochemical Energy, Catalysis and Material Science Laboratory, Department of Chemistry, Technical University Berlin, 10623 Berlin, Germany.*

<sup>b</sup> *Ernst-Ruska Centre for Microscopy and Spectroscopy with Electrons and Peter Grünberg Institute, Forschungszentrum Jülich GmbH, 52425 Jülich, Germany.*

<sup>c</sup> *School of Applied and Engineering Physics, Cornell University, Ithaca, NY 14850, USA.*

*\* Corresponding author email address: [pstrasser@tu-berlin.de](mailto:pstrasser@tu-berlin.de)*

**Table S1** Phase composition as obtained by Rietveld refinement of XRD pattern – values given in weight%.

Sample	PtNi phase 1	PtNi phase 2	Ni phase
PtNi_raw	64.5	6.0	29.5
PtNi_300	63.2	13.8	23.0
PtNi_500	65.5	26.2	8.3

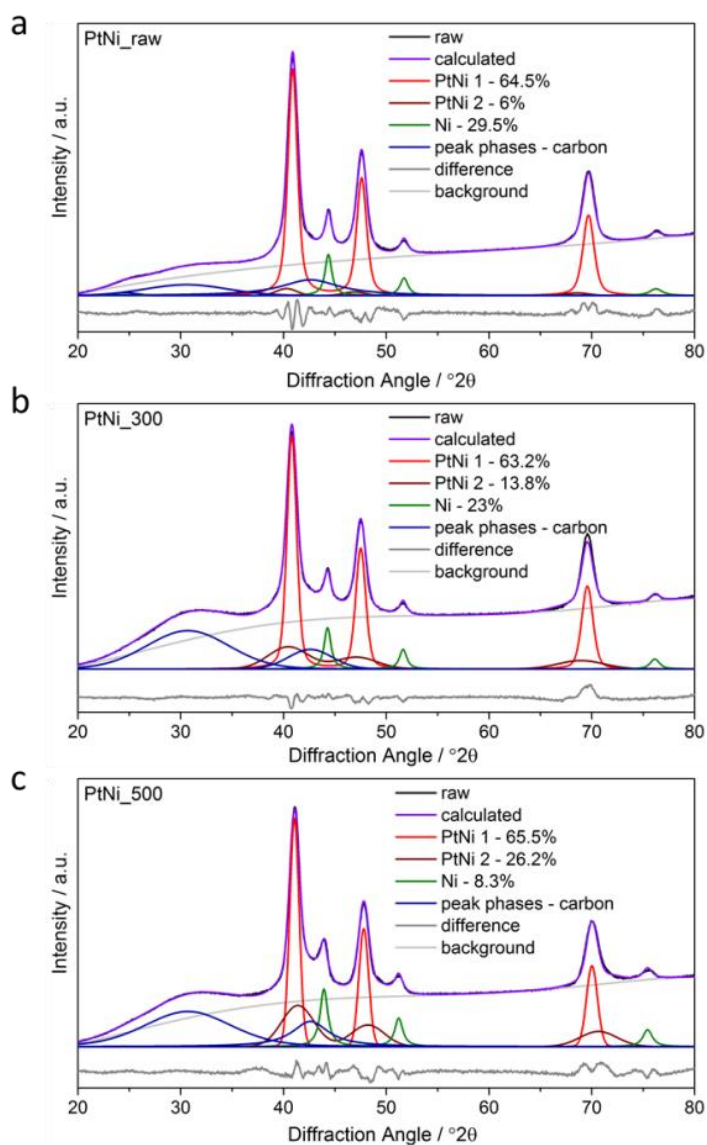


**Figure S1** Rietveld refinement patterns of PtNi\_raw, PtNi\_300 and PtNi\_500.

**Table S2.** Structural parameters obtained by Rietveld refinement of XRD pattern.

Sample	PtNi phase 1		PtNi phase 2		Ni phase		Rwp
	a	LVol-IB	a	LVol-IB	a	LVol-IB	
PtNi_raw	3.7707(24)	7.79	3.7783(34)	2.458(68)	3.4891(22)	7.85(22)	1.06
PtNi_300	3.7770(35)	7.30(52)	3.8060(65)	1.97(11)	3.4951(33)	8.76(40)	1.28
PtNi_500	3.7551(26)	8.493(53)	3.7256(31)	2.424(69)	3.5218(24)	7.45(25)	1.12

**Details to Rietveld Refinement:**

- background: Chebychev with 4/5 polynomial coefficients
- phases:
  - two Pt fcc with Pt and Ni sites
    - phase 1: Pt and Ni occupancy was applied according to composition 0.6 and 0.4, respectively
    - phase 2: Pt and Ni occupancy was refined
  - one Ni fcc
  - additional peak phases to subtract carbon support or influence of holder:  $24.98^{\circ}2\theta$  ,  $30.37^{\circ}2\theta$  and  $43.2^{\circ}2\theta$

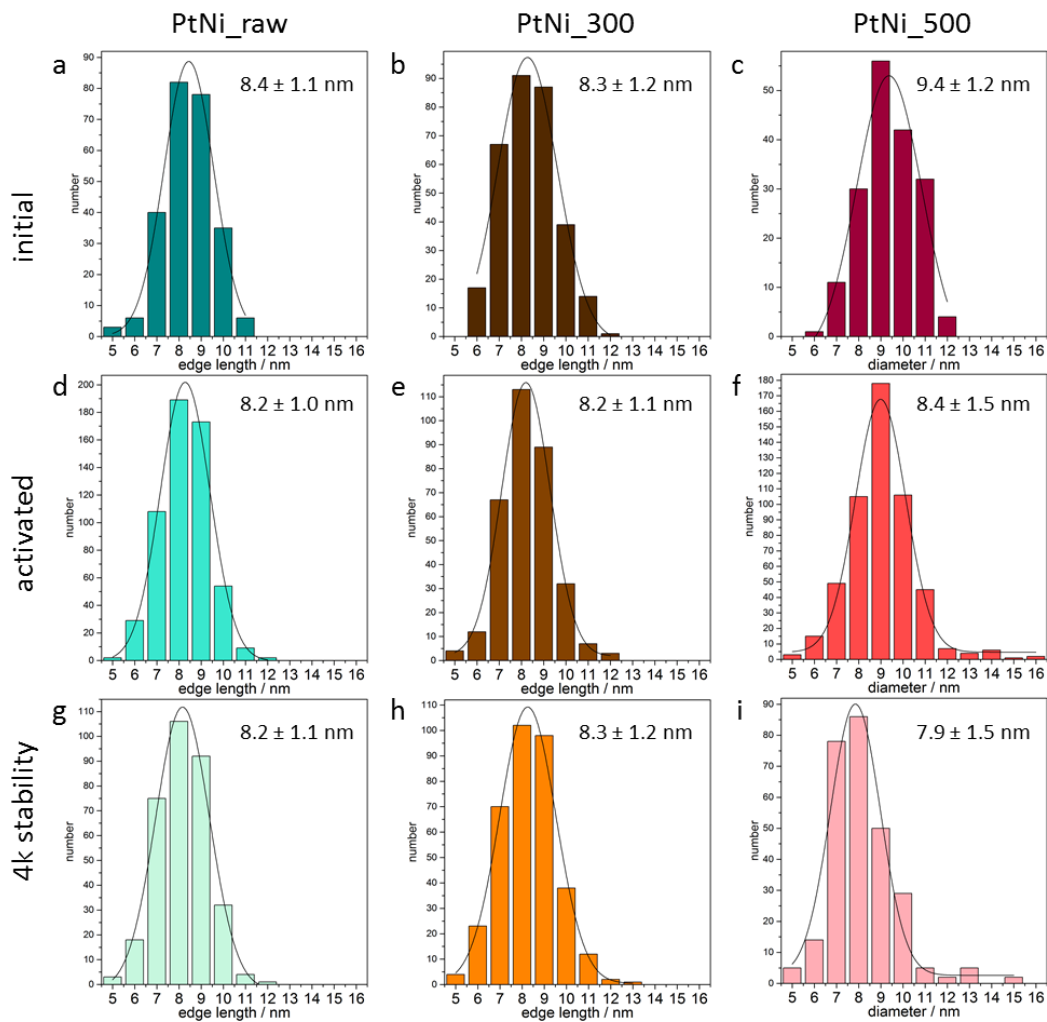


**Figure S2** Particle size distribution of *PtNi\_raw* (a, d, g), *PtNi\_300* (b, e, h) and *PtNi\_500* (c, f, i) in the initial state, after activation and after 4k stability test with the corresponding Gaussian fit.

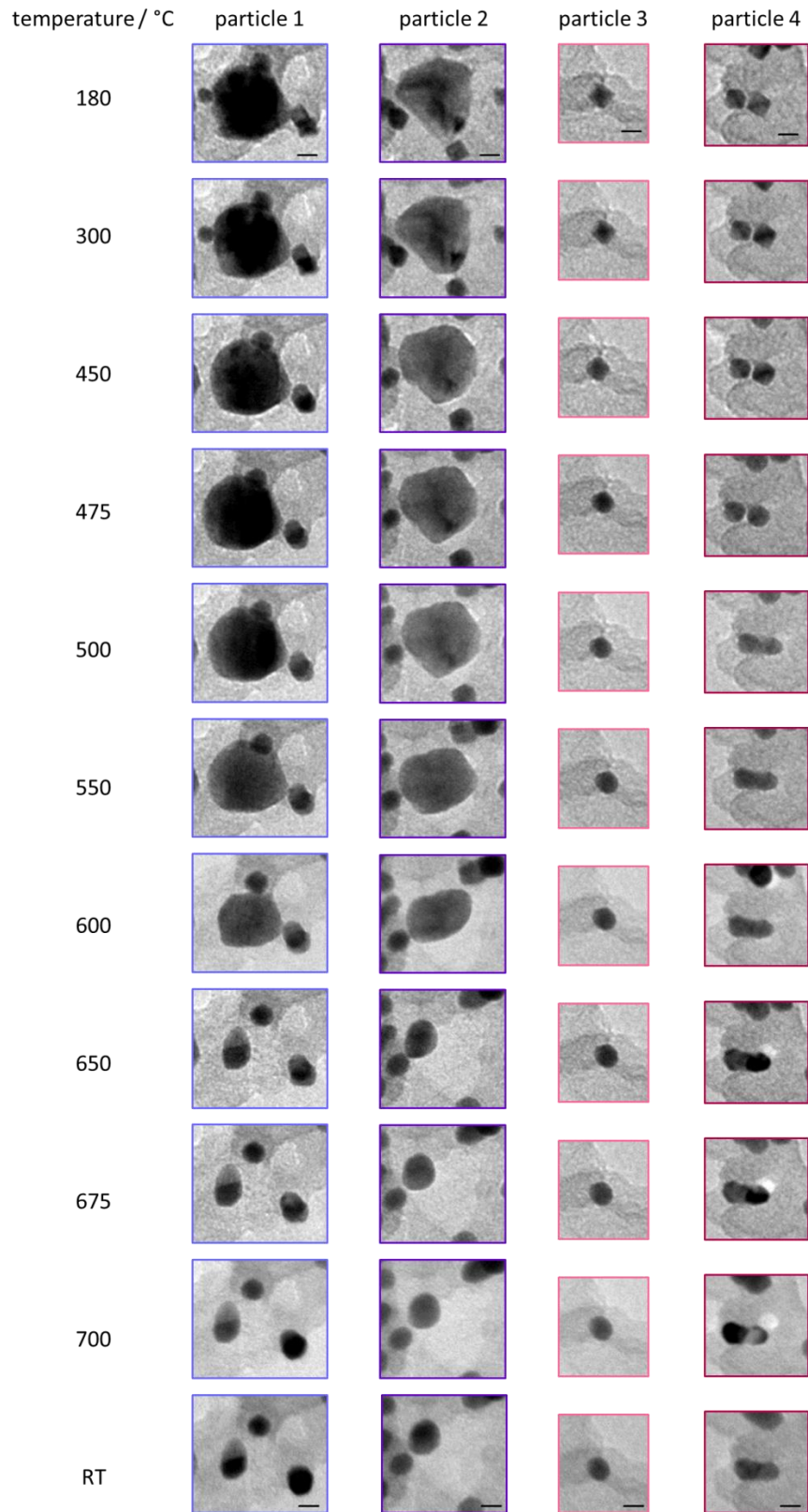


**Figure S3** *In situ* heating TEM images selected from Figure 2. Selected images enlarged for improved disclosure of changes in nanoparticle shape. Scalebars: 10 nm.

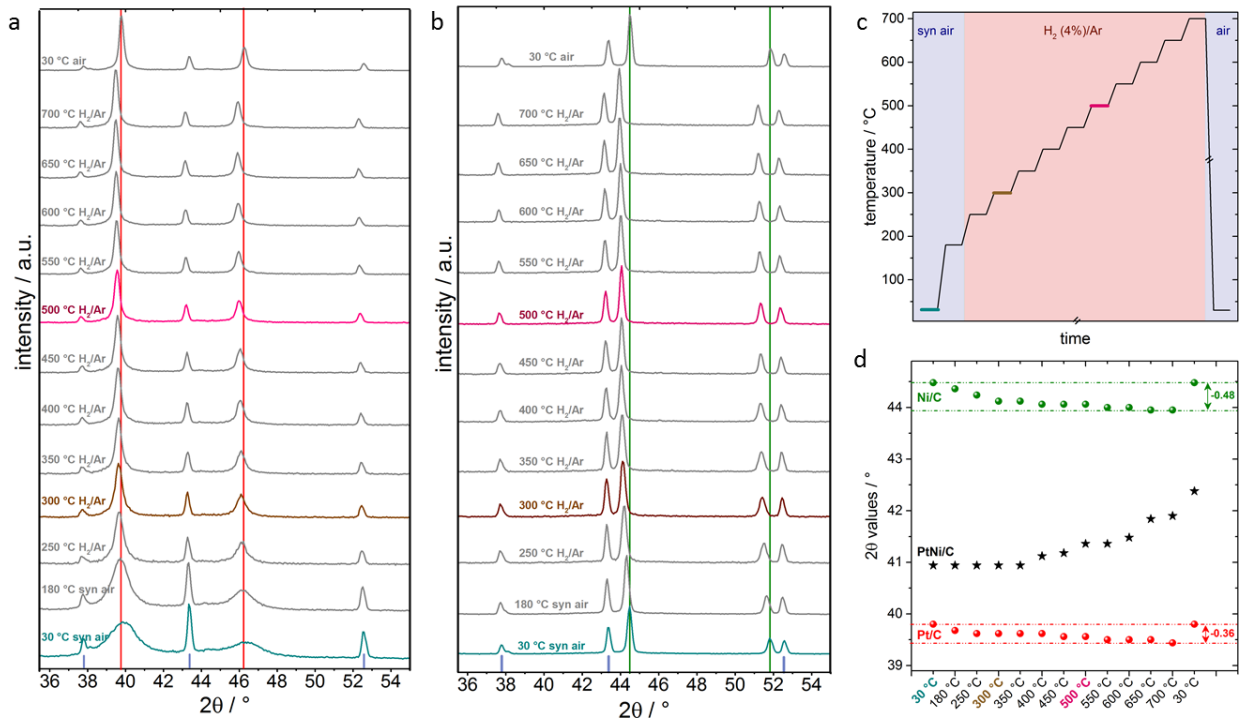


**Figure S4** *In situ* heating x-ray diffractograms of the (111) and (200) signals in the temperature range between 30 °C and 700 °C. Gas atmospheres were chosen comparably to the *ex situ* annealing conditions in the tube furnace and temperature range was chosen according to the *in situ* heating TEM experiment. (a) *in situ* heating XRD of Pt/C (fcc), (b) *in situ* heating XRD of Ni/C (fcc), red columns are assigned to pure Pt peaks, greens columns to pure Ni and blue to  $\text{Al}_2\text{O}_3$  caused by the sample holder. (c) Temperature profile and gas atmospheres of the heating experiment; the whole *in situ* XRD experiment lasted 25 hours including delay time for purging gas and holding temperatures. (d) Shift of the (111) peak maximum with different temperatures of Pt/C (red squares), Ni/C (green squares) and Pt-Ni/C (black stars).

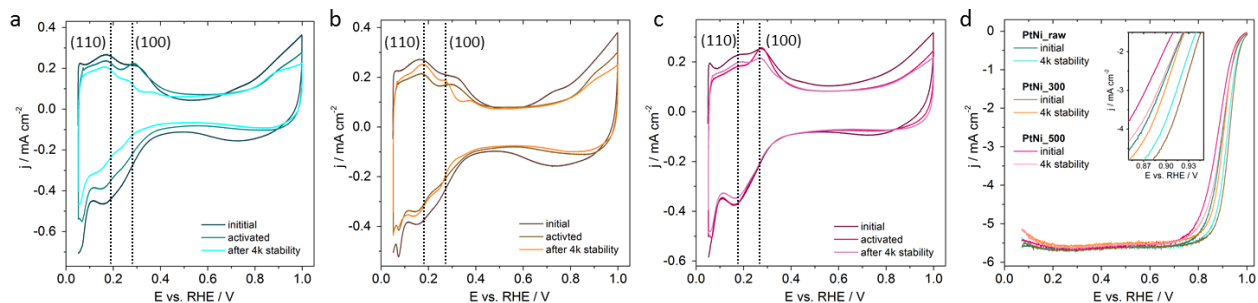


**Figure S5** Electrochemical surface characterization and activity measurement of octahedral Pt-Ni/C; (a-c) cyclic voltammograms (CVs) with  $H_{\text{upd}}$  region after no electrochemical pre-treatment (initial), activation (activated) and 4k stability testing (4k stability); (d) linear sweep voltammetry of the three materials after activation and after 4k cycles stability test.  $H_{\text{upd}}$  CVs were measured between 0.05 and 1.0  $V_{\text{RHE}}$  with  $100 \text{ mV s}^{-1}$  and 4k stability measurements were measured between 0.5 and 1.0  $V_{\text{RHE}}$  with  $50 \text{ mV s}^{-1}$  in  $\text{N}_2$  sat. 0.1 M  $\text{HClO}_4$  and 0 rpm; LSVs were measured in  $\text{O}_2$  sat. 0.1 M  $\text{HClO}_4$  between 0.05 and 1.0  $V_{\text{RHE}}$  with  $5 \text{ mV s}^{-1}$ , 1600 rpm and were iR corrected.

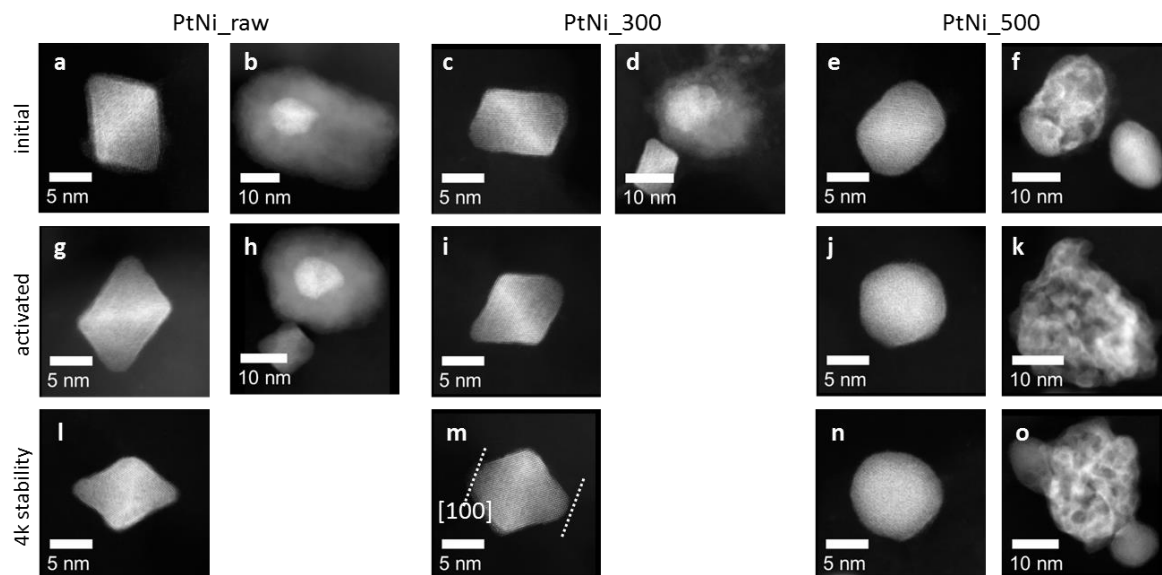


**Figure S6** HAADF STEM images of *PtNi\_raw* (a, b, g, h, l), *PtNi\_300* (c, d, i, m) and *PtNi\_500* (e, f, j, k, n, o) in the initial condition (a and b, c and d, e and f), after activation (g and h, i, j and k) and after 4k stability test (l, m, n and o). If present, also bigger mostly Ni-rich particles are depicted (b and h, d, f and k and o).

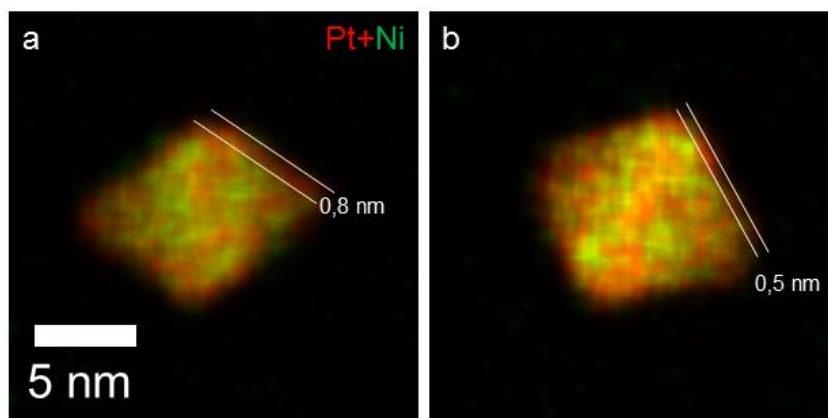


**Figure S7** EDX elemental maps showing the composition of *PtNi\_raw* (a) and *PtNi\_300* (b) after 4k stability test. Pt: red and Ni: green.

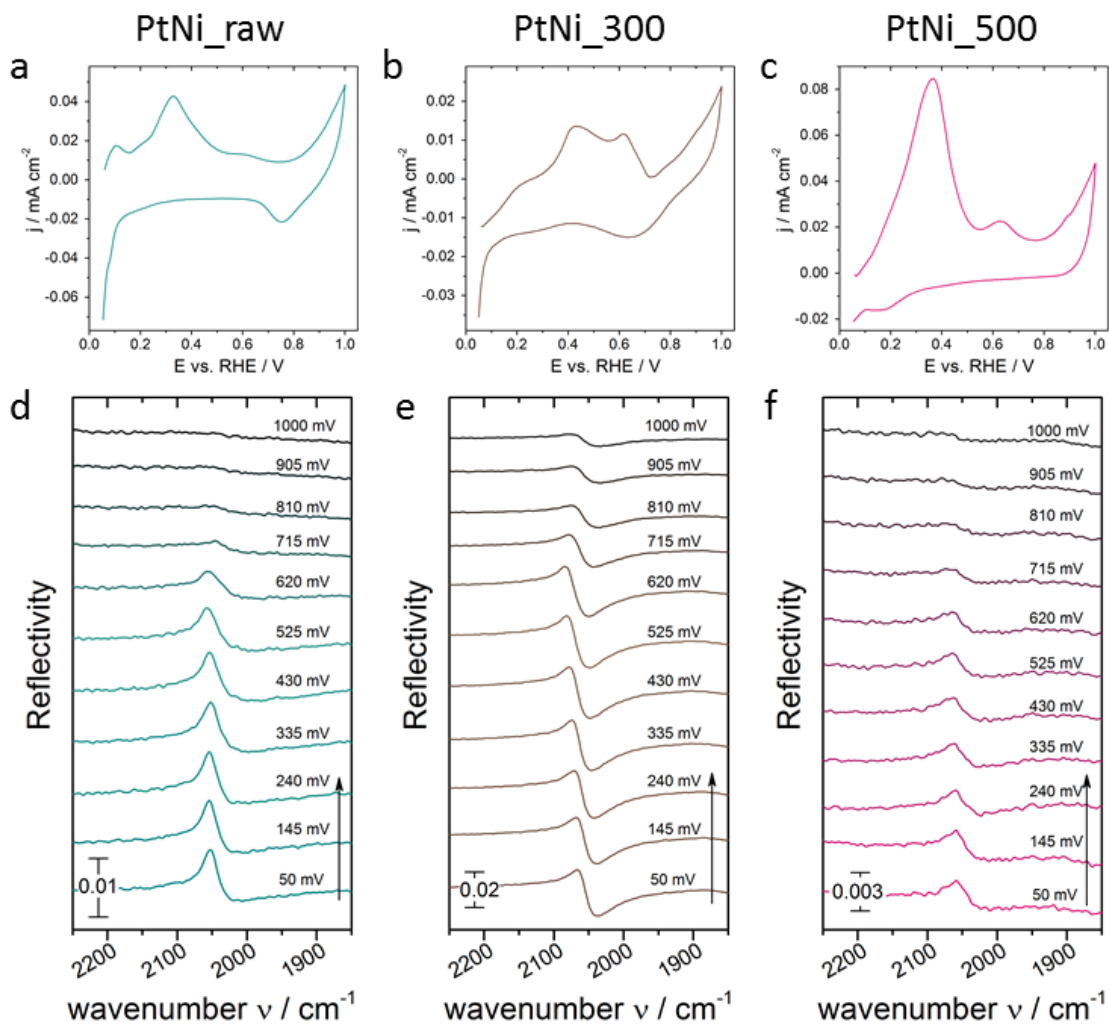
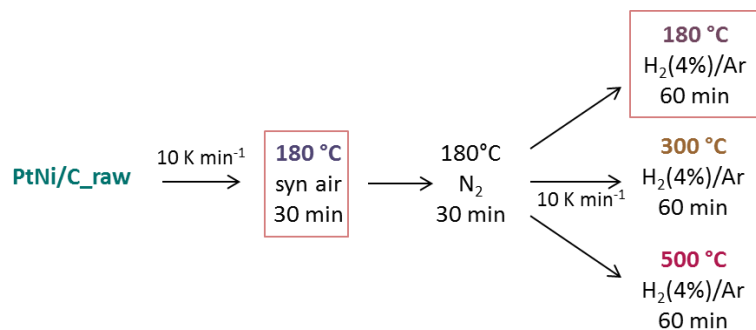


**Figure S8** Representative sets of ATR FTIR reflectivity spectra of the catalyst surface during electrochemical CO oxidation with corresponding electrochemical curves. *PtNi\_raw* (a, d), *PtNi\_300* (b, e) and *PtNi\_500* (c, f) are shown after electrochemical activation (20 cycles). The potential was scanned from 50 to 1000 mV<sub>RHE</sub> and back (not shown) with a scan rate of 1 mV s<sup>-1</sup> in 0.1 M HClO<sub>4</sub>. An IR spectra is represented every 95 mV. The background spectrum was taken before adding CO at a constant potential of 50 mV<sub>RHE</sub>.



**Scheme S1** Overview of post-synthesis treatments including acetic acid treatment and annealing protocols. Newly added samples are marked with red squares.

An additional set of PtNi particles was synthesized as shown in Scheme S1 and tested in terms of their characteristics, comparable to the particles discussed in the main manuscript. As these samples descending from a different batch of particles than the previously discussed once, they are marked with PtNi\*\_raw, PtNi\*\_air and PtNi\*\_180.

X-ray diffraction patterns show no significant change after annealing at 180 °C (Figure S9). The same is true for the electrochemical characteristics. The ORR activities and ECSA (Figure S10 a,b) values are all within the error, CO stripping profiles (Figure S10 c-e) and cyclic voltammetry (Figure S11 a-c) show no remarkable differences. We also performed FTIR spectroscopy on the three samples using CO as a surface probe molecule adsorbed on the particle surface at 50 mV<sub>RHE</sub>. The CO stretching vibrations all appear at roughly the same wavenumber (Figure S12) and the corresponding *in situ* CO stripping profiles (Figure S13) show the same redox feature for all three samples.

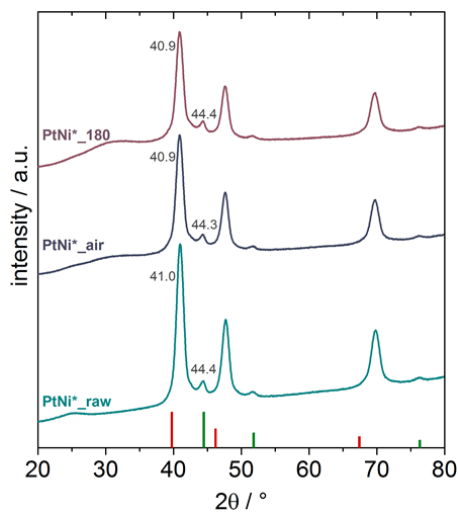


**Figure S9** XRD pattern of *PtNi\_raw*, *PtNi\_180\_air* and *PtNi\_180*. Red columns correspond to pure Pt (PDF#00-004-0802) peaks and green columns to pure Ni (PDF#00-004-0850).

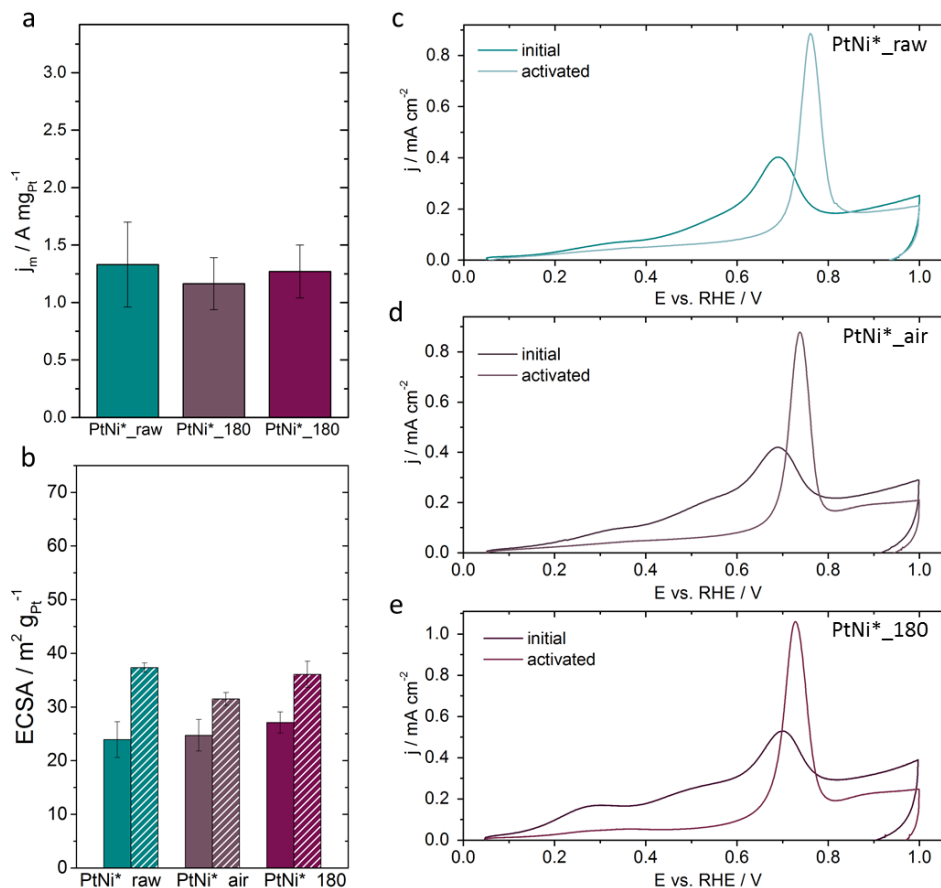


**Figure S10** (a) Electrochemical ORR activity of the activated state (after 20 cyclic voltammograms (CV) activation) evaluated at 0.9 V; ORR was measured in  $O_2$  sat. 0.1 M  $HClO_4$  between 0.05 and 1.0  $V_{RHE}$  with  $5\text{ mV s}^{-1}$ , 1600 rpm and were iR corrected (b) Electrochemical active surface area determined by integration of the hydrogen under potential deposition region ( $H_{upd}$ ) (solid colors) and the CO oxidation peak (striped colors) after activation. The error bars depicting the standard deviation between at least three different and independent measurements of freshly prepared catalyst films. (c-e) Positive CO oxidation profile of the initial samples and the activated.  $H_{upd}$  values were evaluated from CVs measured in  $N_2$  sat. 0.1 M  $HClO_4$  between 0.05 and 1.0  $V_{RHE}$  with  $100\text{ mV s}^{-1}$   $H_{upd}$ , CO oxidation was performed in  $N_2$  sat. 0.1 M  $HClO_4$  between 0.05 and 1.0  $V_{RHE}$  with  $50\text{ mV s}^{-1}$  and 0 rpm.

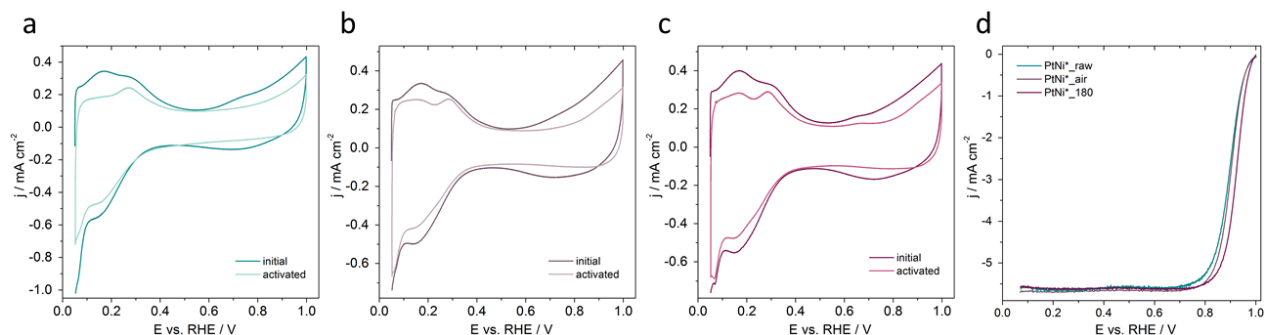


**Figure S11** Electrochemical surface characterization and activity measurement of octahedral Pt-Ni\*/C; (a-c) cyclic voltammograms (CVs) with  $H_{upd}$  region after no electrochemical pre-treatment (initial) and after activation (activated)); (d) linear sweep voltammetry of the three materials after activation.  $H_{upd}$  CVs were measured in  $N_2$  sat. 0.1 M  $HClO_4$  between 0.05 and 1.0  $V_{RHE}$  with  $100\text{ mV s}^{-1}$  and 0 rpm; LSVs were measured in  $O_2$  sat. 0.1 M  $HClO_4$  between 0.05 and 1.0  $V_{RHE}$  with  $5\text{ mV s}^{-1}$ , 1600 rpm and were iR corrected.

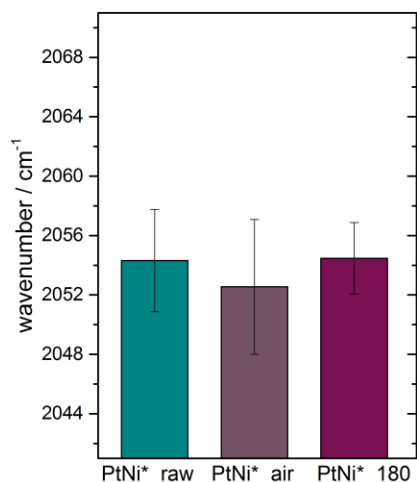


**Figure S12** *In situ* FTIR spectroscopy measured in ATR mode showing the position of CO<sub>ad</sub> band of the linear bounded CO collected at 50 mV<sub>RHE</sub> in N<sub>2</sub> sat. 0.1 M HClO<sub>4</sub> for the different samples after electrochemical activation. The error bars depicting the standard deviation between at least three different and independent measurements of freshly prepared catalyst films.

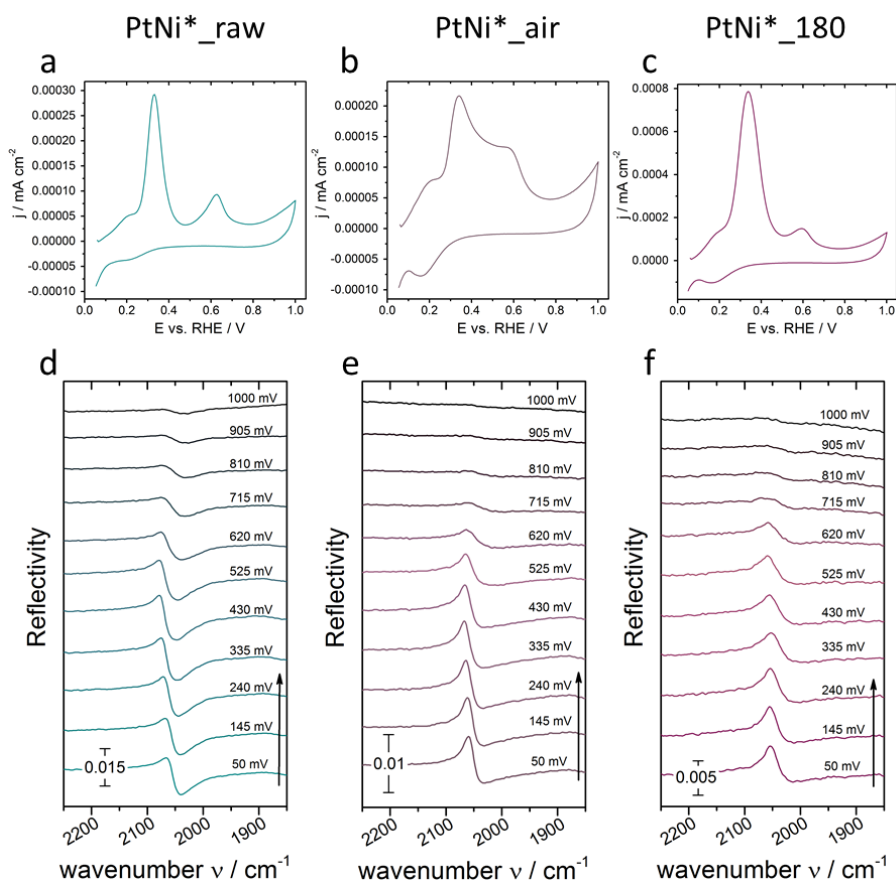


**Figure S13** Representative sets of ATR FTIR reflectivity spectra of the catalyst surface during electrochemical CO oxidation with corresponding electrochemical curves. *PtNi\*\_raw* (a, d), *PtNi\*\_air* (b, e) and *PtNi\*\_180* (c, f) are shown after electrochemical activation (20 cycles). The potential was scanned from 50 to 1000 mV<sub>RHE</sub> and back (not shown) with a scan rate of 1 mV s<sup>-1</sup> in 0.1 M HClO<sub>4</sub>. An IR spectra is represented every 95 mV. The background spectrum was taken before adding CO at a constant potential of 50 mV<sub>RHE</sub>.

Figures S14 and S15 show high angle annular dark field (HAADF) STEM images of PtNi\* nanoparticles in different states and the corresponding EDX composition maps.

For the octahedral PtNi\*\_raw nanoparticle, oriented close to the  $\langle 110 \rangle$  zone axis, the EDX map indicates an enrichment of Ni at the  $\{111\}$  facets, a Pt-rich frame, which is pointed out by a Pt-rich strip in the middle of the nanoparticle, and a Ni rich shell surrounding the octahedral nanoparticle (Figure S14c). EDX quantification yields an average composition of Pt 52 at.% and Ni 48 at.% for particles in the initial state. However, for the PtNi\*\_180 and PtNi\*\_air particles no significant difference in the elemental distribution nor in the composition is visible. For PtNi\*\_180 the average composition is Pt 52 at.%, Ni 48 at.% and for PtNi\*\_air Pt 48 at.%, Ni 52 at.%, respectively (Figure 4).

After activation, EDX quantification yields an average composition of Pt 69 at.% and Ni 31 at.% for PtNi\*\_raw, Pt 72 at.% and Ni 28 at.% for PtNi\*\_180 and an average composition of Pt 68 at.%, Ni 32 at.% for PtNi\*\_air after 20 CV (Figure S15). Thus Ni dissolution is visible after electrochemical cycling in acidic solution. For PtNi\*\_raw, PtNi\*\_180 and PtNi\*\_air the EDX maps indicate the removal of the former Ni rich shell. Further in the EDX maps a thin Pt layer is observed at the outermost parts of the octahedra, which might be due to the presence of Pt-rich edges or the formation of a thin Pt-rich skin on the facets of the octahedra. Hence, also here no significant change for PtNi\*\_raw, PtNi\*\_180 and PtNi\*\_air in elemental distribution and composition is visible.

In addition to the octahedral nanoparticles, again bigger irregular-shaped nanoparticles are observed (Figures S14 d,e, i, j, n, o and S15 d,e, i, j, n, o). The irregular-shaped nanoparticles consist always of a Pt rich nanoparticle which is encased by Ni. The overall average composition of the bigger nanoparticles is Pt 3 at.%, Ni 97 at.% for PtNi\*\_raw, PtNi\*\_180 and PtNi\*\_air. After 20 CV the bigger irregular nanoparticles are also found with no significant changes in composition and elemental distribution.

Thus, the 180 °C air annealed and 180 °C H<sub>2</sub>/Ar annealed samples exhibit the same characteristics like the as prepared sample. Accordingly, PtNi\_raw is suitable to be discussed as starting material for this study.

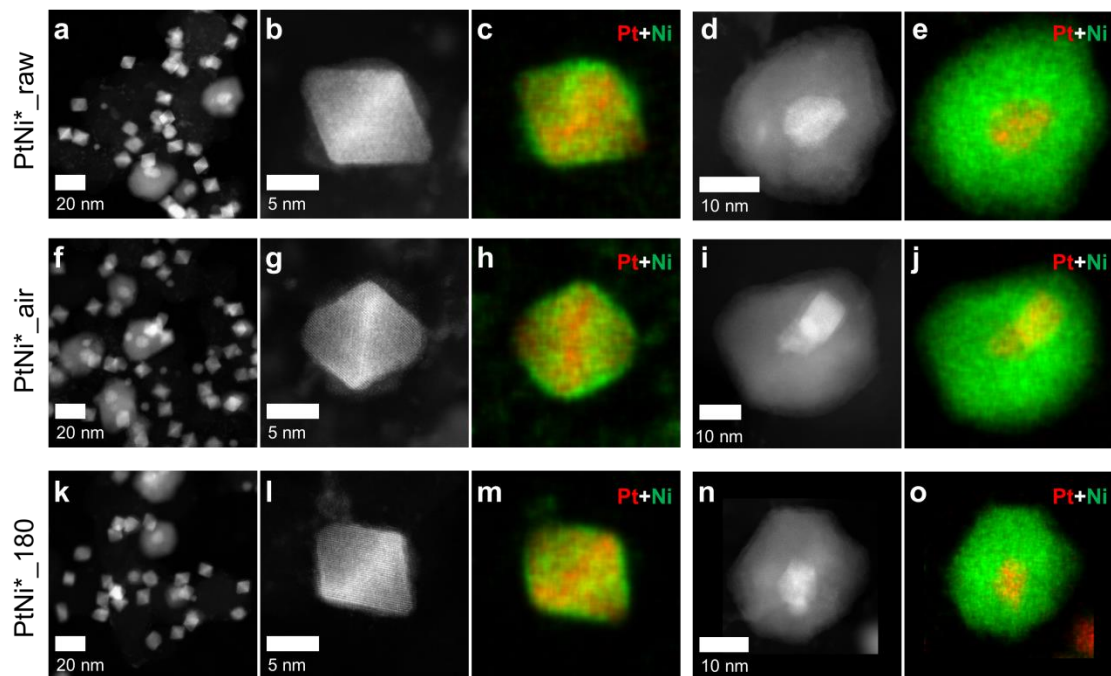


**Figure S14** HAADF images and EDX elemental maps of the *initial PtNi\*\_raw (a-e), PtNi\*\_air (f-j) and PtNi\*\_180 (k-o)*. Octahedral and big irregular shaped Ni-rich particles are shown. Pt: red and Ni: green. Particle shape and size and elemental distribution show no remarkable difference between the samples. All samples are also comparable to PtNi\_raw discussed in the main manuscript.

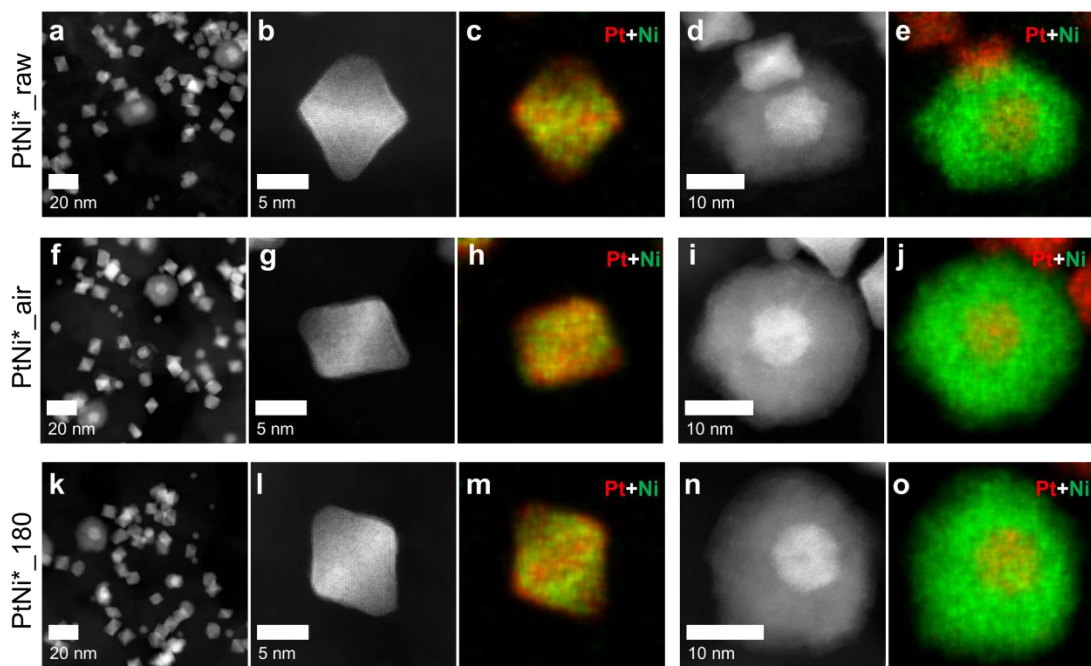


**Figure S15** HAADF images and EDX elemental maps of the *activated PtNi\*\_raw (a-e), PtNi\*\_air (f-j) and PtNi\*\_180 (k-o)*. Octahedral and big irregular shaped Ni-rich particles are shown. Pt: red and Ni: green. Particle shape and size and elemental distribution show no remarkable difference between the samples. All samples are also comparable to PtNi\_raw discussed in the main manuscript.